Supplement of Geosci. Model Dev., 18, 6479–6515, 2025
https://doi.org/10.5194/gmd-18-6479-2025-supplement
© Author(s) 2025. CC BY 4.0 License.



Geoscientific Model Development
Open Access
EGU

Supplement of

Implementation of the MOSAIC aerosol module (v1.0) in the Canadian air quality model GEM-MACH (v3.1)

Kirill Semeniuk et al.

Correspondence to: Kirill Semeniuk (kirill.semeniuk@ec.gc.ca)

The copyright of individual parts of the supplement might differ from the article licence.

S1. Model-Observation Correlation Analysis

Model-observation correlation plots are presented here for all four model simulations for monthly-binned daily PM2.5 sulfate, nitrate and ammonium. Observational data is from station networks referenced in the article: CSN, IMPROVE and NAPS.

Figures S1-S3 show results for the MOSAIC reference simulation. Figures S4-S6 are for the CAM reference simulation. Simulations with Emerson et al. (2020) dry deposition parameters with MOSAIC are shown in Figures S7-S9 and with CAM in Figures S10-S12.

For sulfate, the reference CAM and MOSAIC results are very similar. The largest scatter occurs in winter and spring (January-April and December). There is a tendency for model sulfate to have progressively smaller values than observations as the concentration decreases towards 0.1 $\mu g/m^3$. The low bias in MOSAIC compared to CAM noted in the main article is also apparent.

In the case of CAM, the nitrate deviation to excessively low values for concentrations approaching 0.1 $\mu g/m^3$ is striking. It is most prominent from March to October. In the case of MOSAIC, this deviation is substantially reduced and there is much less scatter. However, MOSAIC has a high bias relative to observations during most months.

For ammonium, CAM and MOSAIC show the same trend to excessively high values as concentrations decrease to 0.1 $\mu g/m^3$. At many station locations, the model concentrations remain above 0.1 $\mu g/m^3$ when observed values approach 0.01 $\mu g/m^3$. Both aerosol schemes show a high bias in the full concentration range for every month of the year. But MOSAIC has a reduced high bias compared to CAM.

MOSAIC with Emerson dry deposition parameters result in a decrease in the bias relative to observations for sulfate and nitrate (Figs. S1-S2 vs. Figs. S7-S8). The modest sulfate low bias is essentially removed. The much more pronounced nitrate high bias is substantially reduced. For ammonium (Fig. S3 vs. Fig. S9) there is an increase in the high bias. The change in the dry deposition parameters does not affect the low bias at small concentrations which appears as a skew towards the observation axis for sulfate and nitrate, and as a skew towards the model axis for ammonium.

The effect of the Emerson parameters on CAM sulfate, nitrate and ammonium (Figs. S4-S6 vs. Figs. S10-S12) is to marginally increase concentrations in the low end of the range and to decrease them in the high end of the range. This is most apparent in fall, winter and spring months. This indicates that low concentrations have a higher association with smaller particle sizes and vice versa.

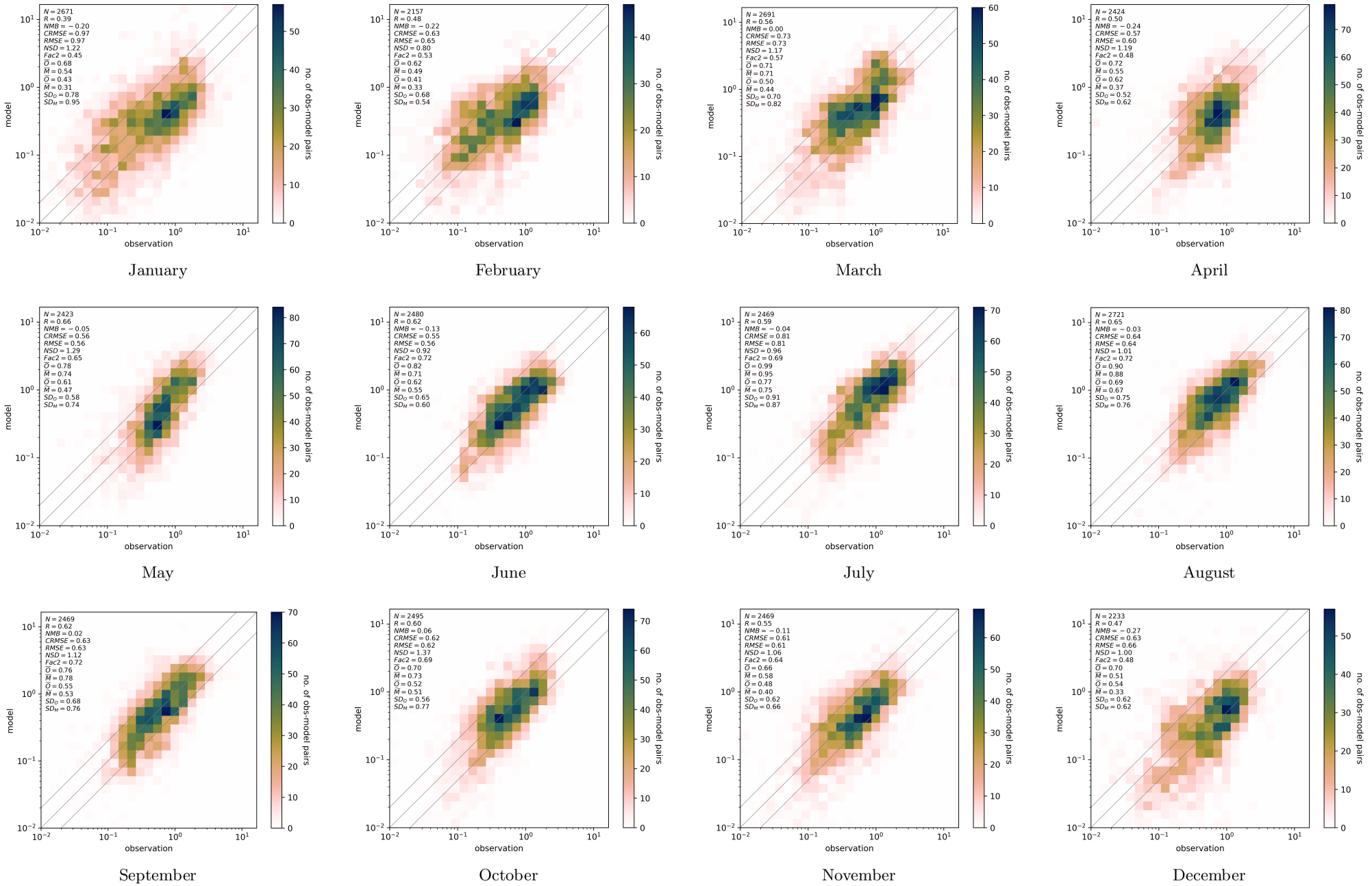


Figure S1: REF MOSAIC Daily PM2.5 SO_4 ($\mu g/m^3$) CSN + IMPROVE + NAPS

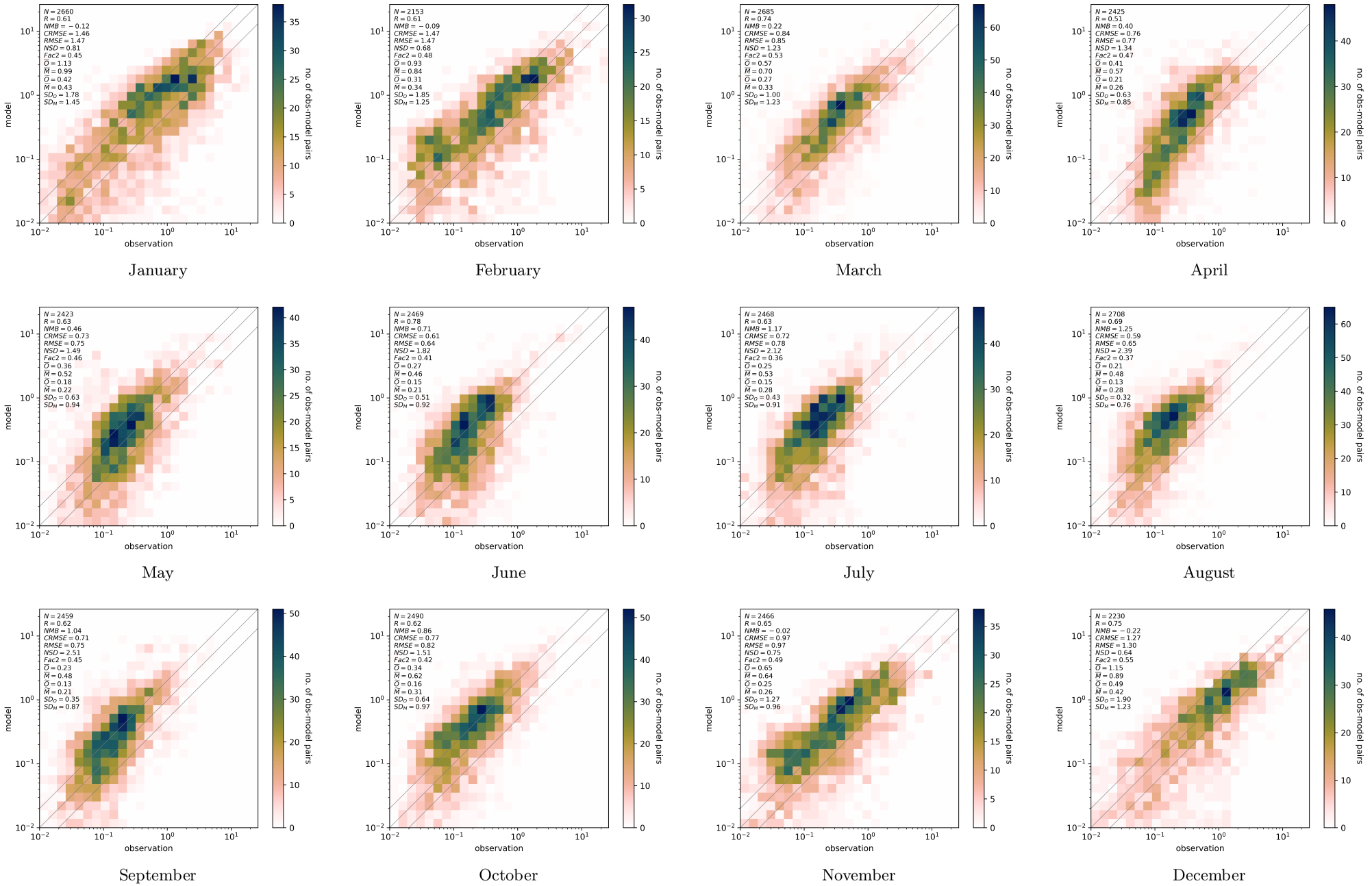


Figure S2: REF MOSAIC Daily PM2.5 NO_3 ($\mu g/m^3$) CSN + IMPROVE + NAPS

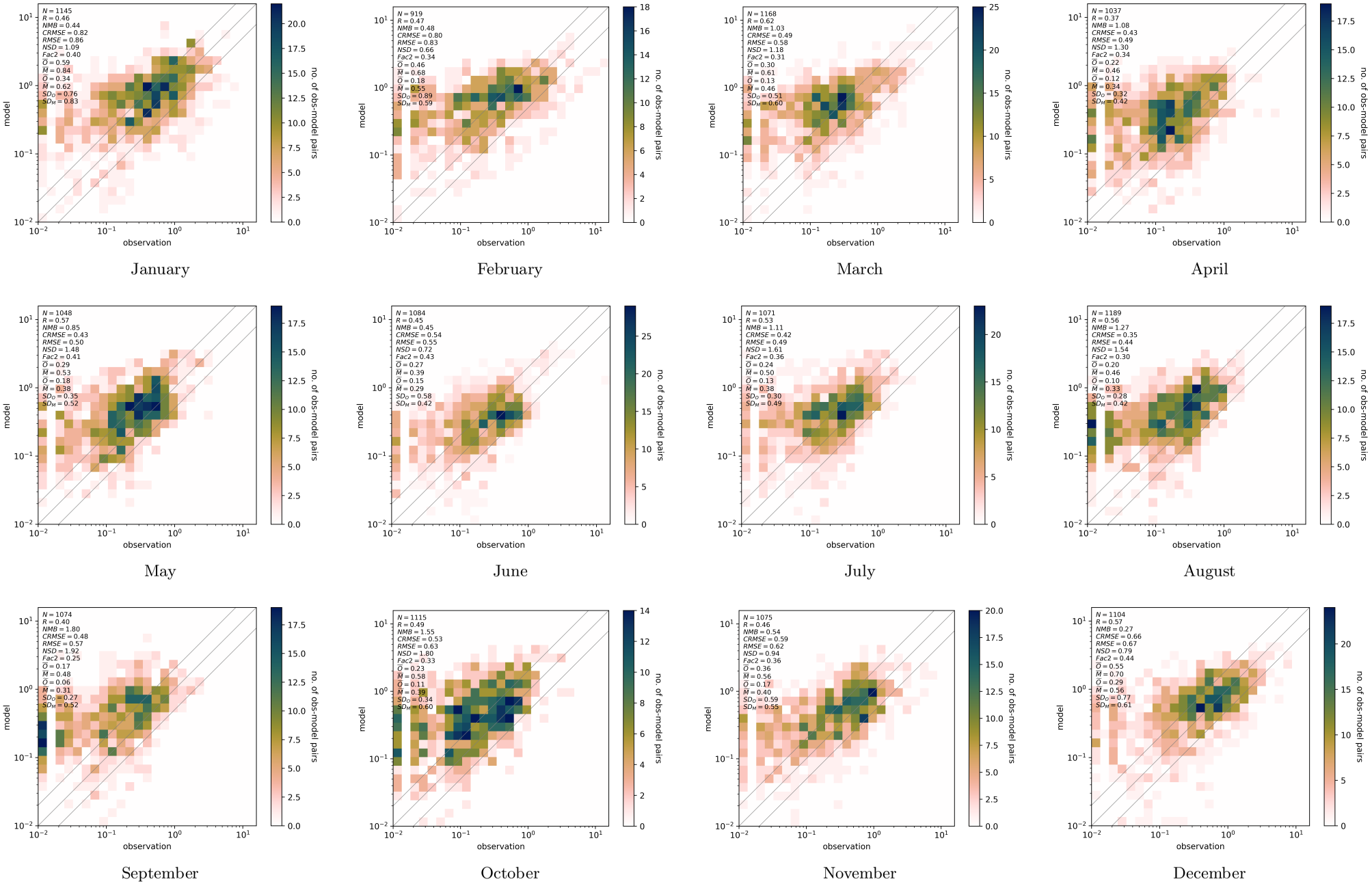


Figure S3: REF MOSAIC Daily PM2.5 NH_4 ($\mu g/m^3$) CSN + NAPS

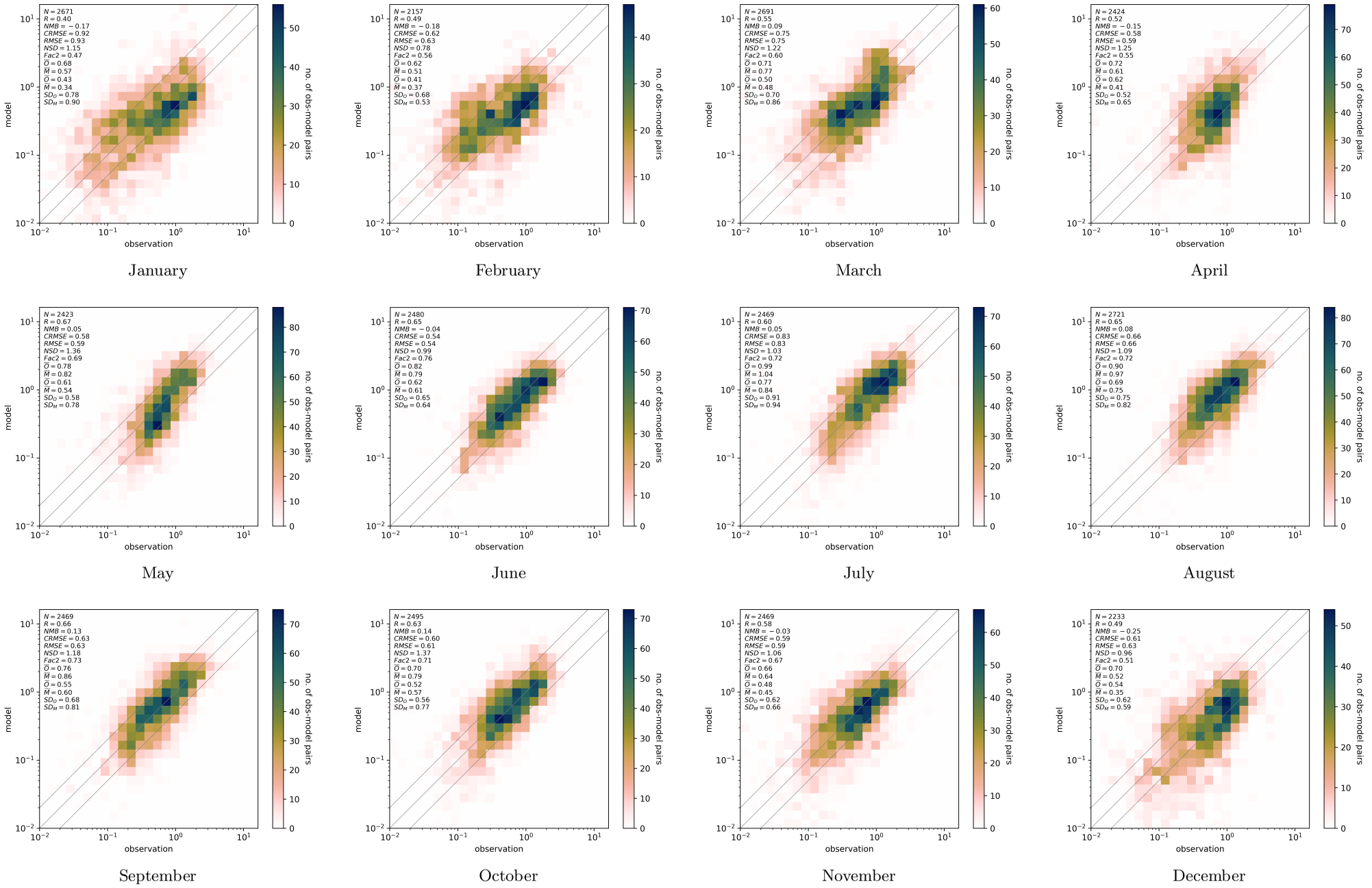


Figure S4: REF CAM Daily PM2.5 SO_4 ($\mu g/m^3$) CSN + IMPROVE + NAPS

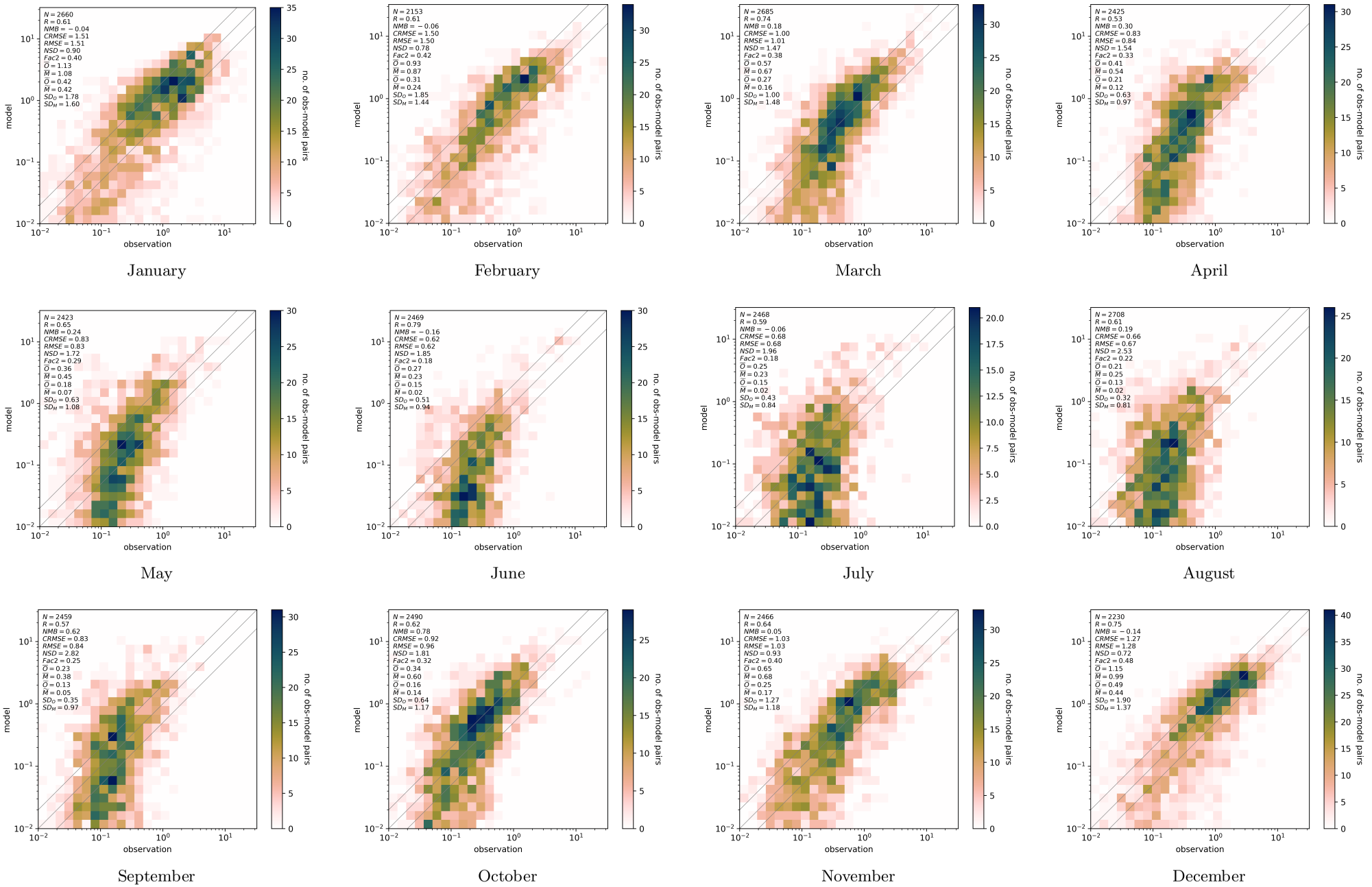


Figure S5: REF CAM Daily PM2.5 NO_3 ($\mu g/m^3$) CSN + IMPROVE + NAPS

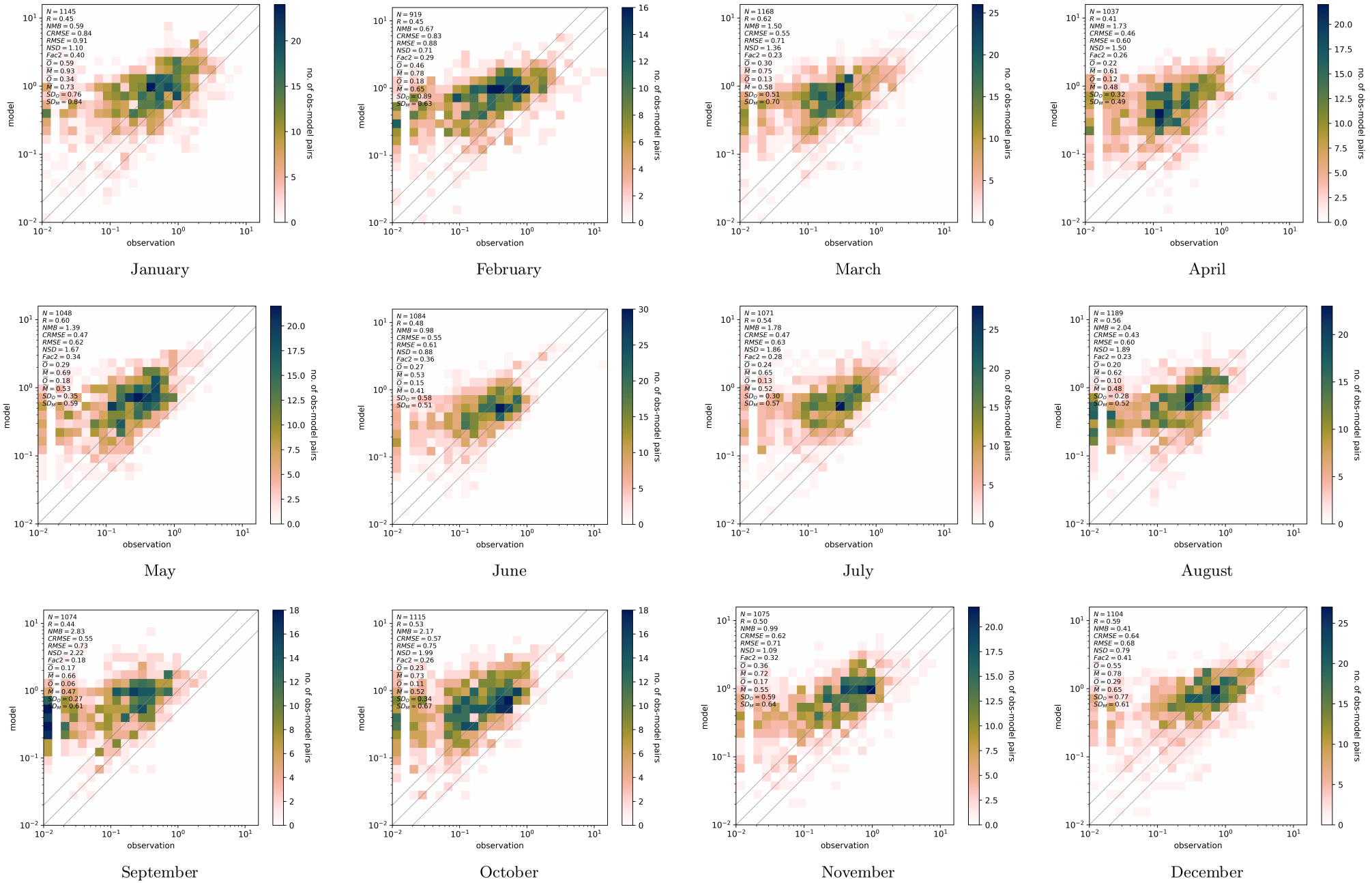


Figure S6: REF CAM Daily PM2.5 NH_4 ($\mu g/m^3$) CSN + NAPS

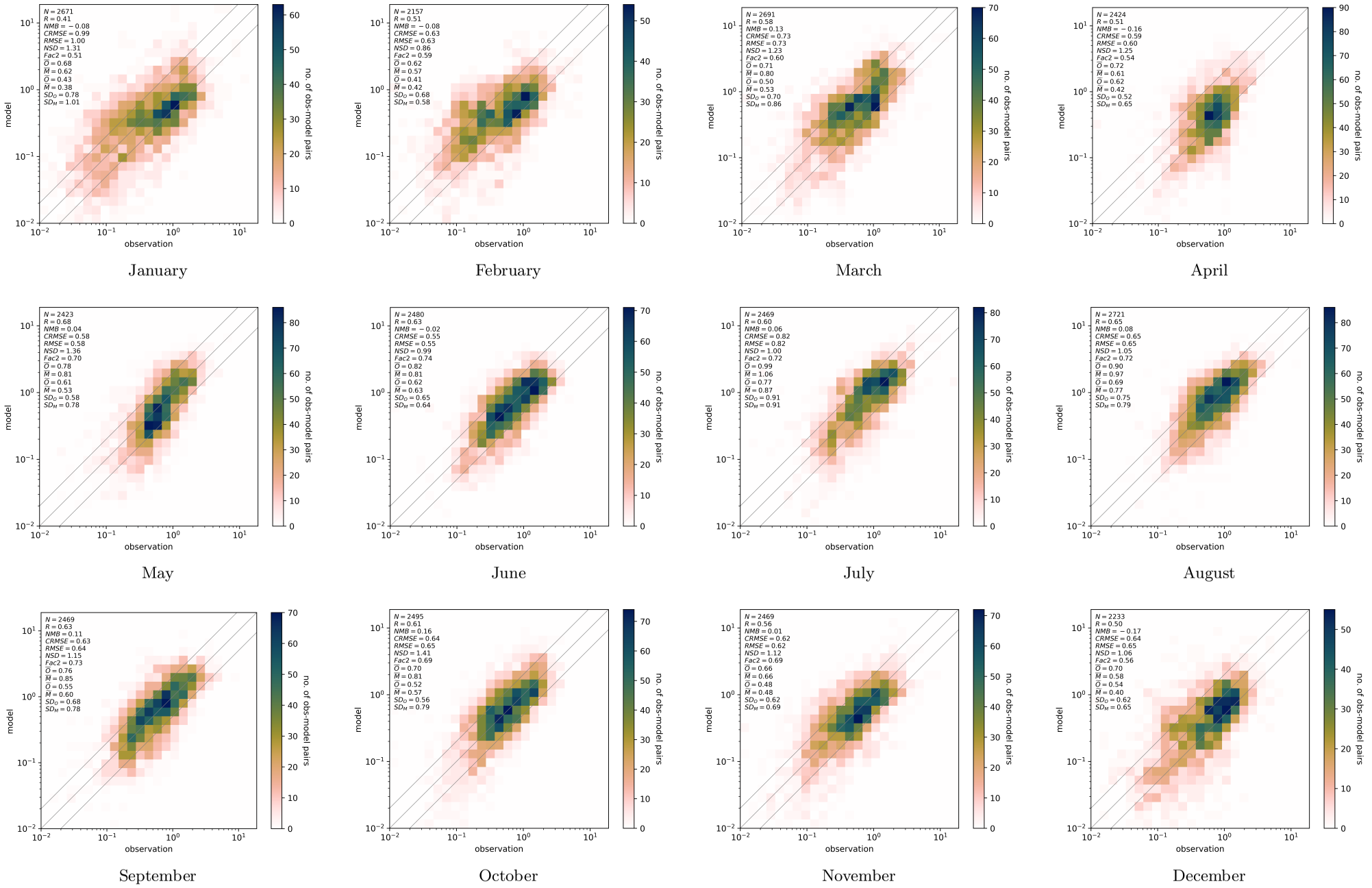


Figure S7: EMR MOSAIC Daily PM2.5 SO_4 ($\mu g/m^3$) CSN + IMPROVE + NAPS

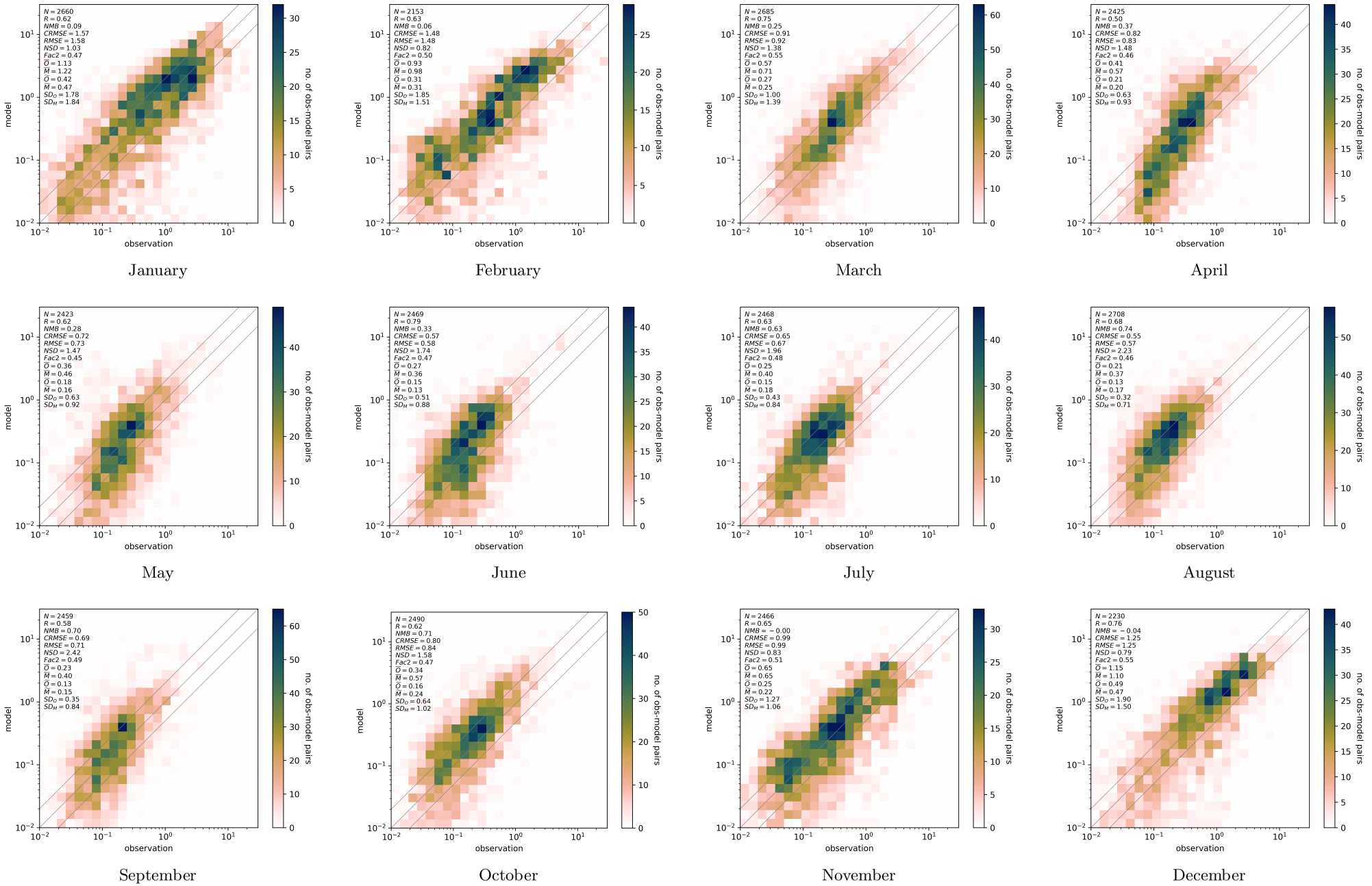


Figure S8: EMR MOSAIC Daily PM2.5 NO_3 ($\mu g/m^3$) CSN + IMPROVE + NAPS

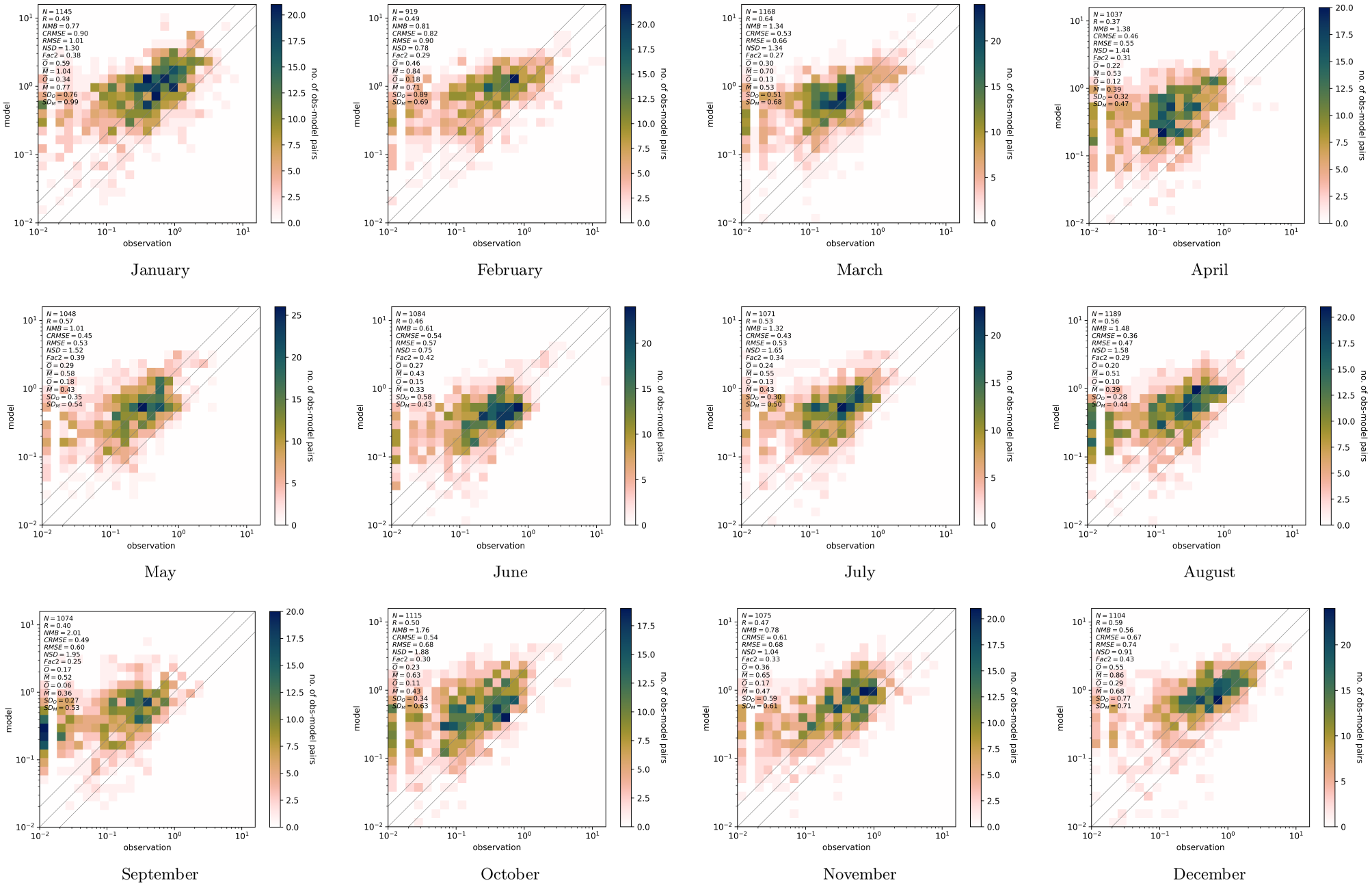


Figure S9: EMR MOSAIC Daily PM2.5 NH_4 ($\mu g/m^3$) CSN + NAPS

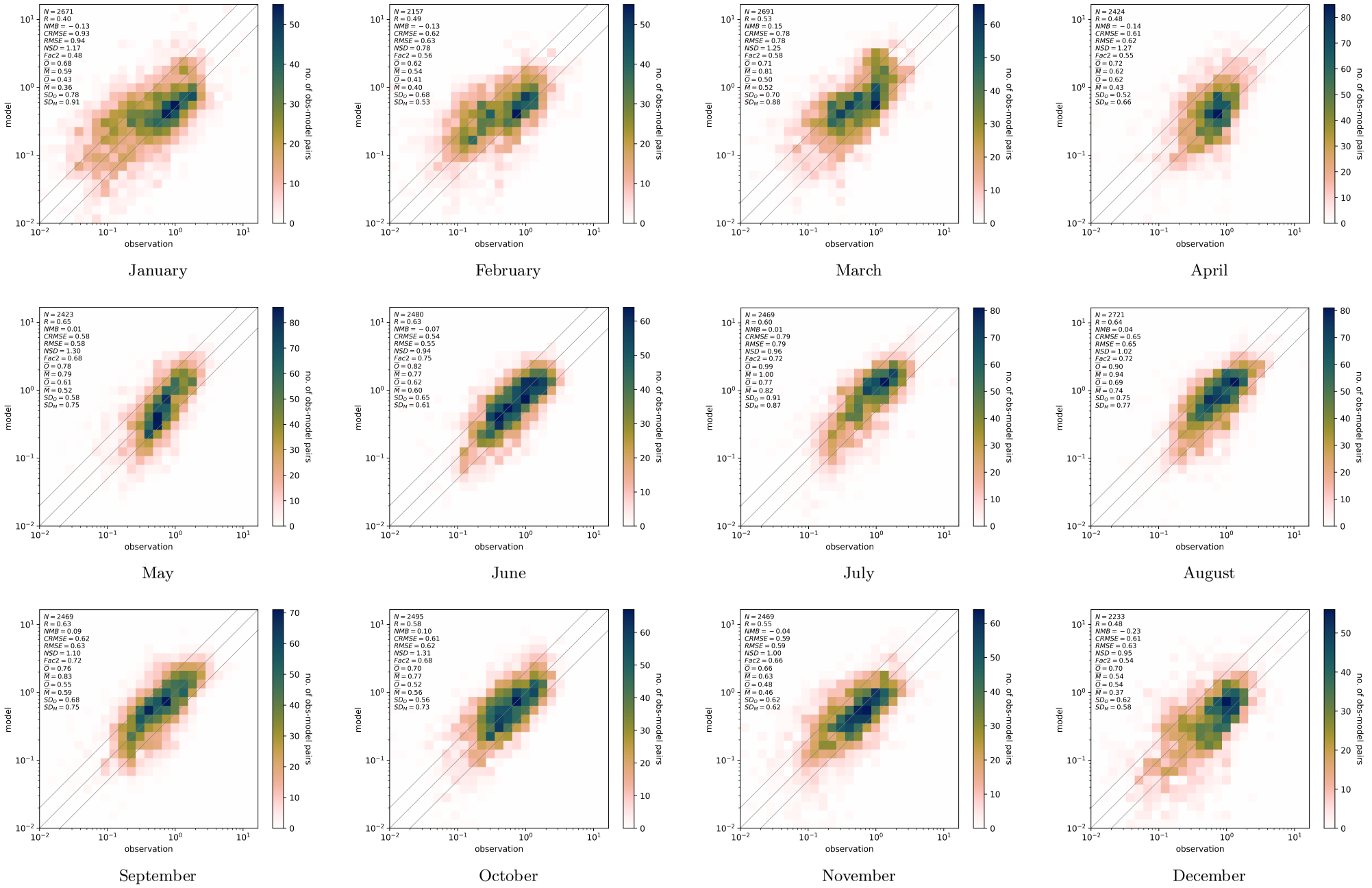


Figure S10: EMR CAM Daily PM2.5 SO_4 ($\mu g/m^3$) CSN + IMPROVE + NAPS

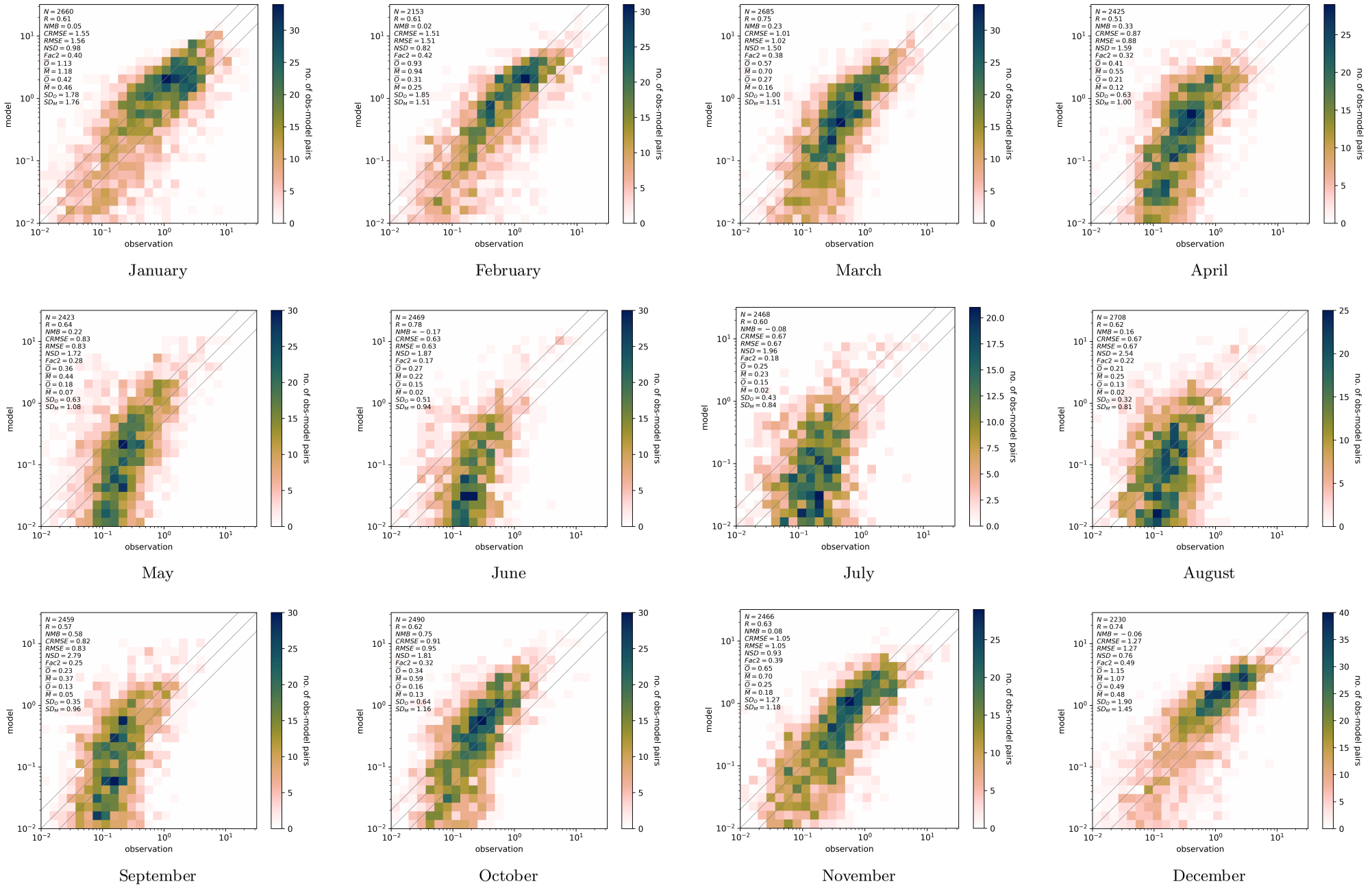


Figure S11: EMR CAM Daily PM2.5 NO_3 ($\mu g/m^3$) CSN + IMPROVE + NAPS

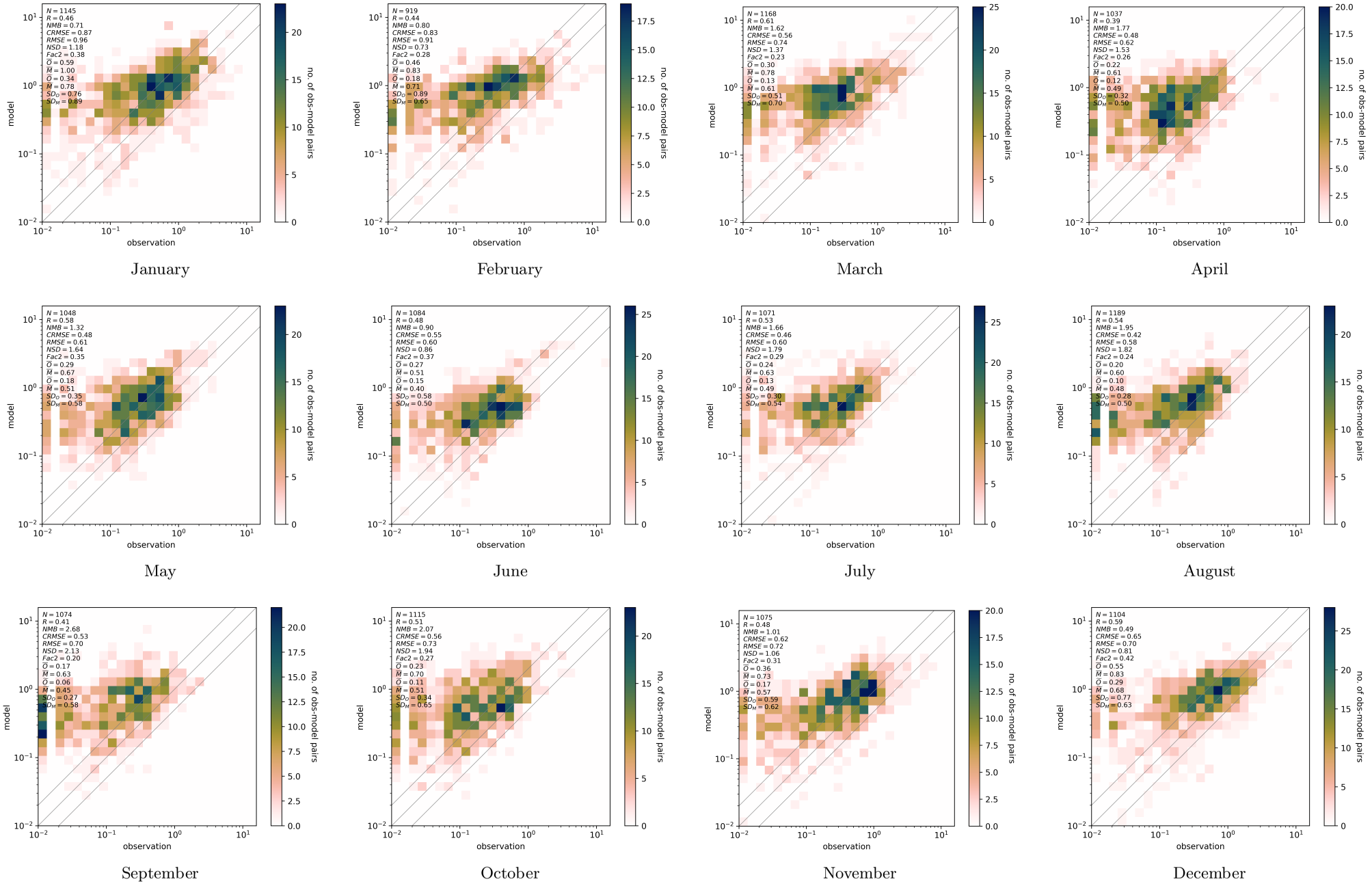


Figure S12: EMR CAM Daily PM2.5 NH_4 ($\mu g/m^3$) CSN + NAPS

S2. Gas Phase Chemical Species Comparison Between Model and Station Observations.

The reference case MOSAIC and CAM monthly and station average NH_3, HNO_3, SO_2, O_3 and NO_x for the four regions defined in the article text (Fig. 9 in the article) are presented in Figure S13. Nitric acid observations are combined from the Clean Air Status and Trends Network (CASTNET, https://www.epa.gov/castnet) and the Canadian Air and Precipitation Network (CAPMoN, https://www.canada.ca/en/environment-climate-change/services/air-pollution/monitoring-networks-data/canadian-air-precipitation.html). Ammonia observations are combined from the Ammonia Monitoring Network (AMON, https://nadp.slh.wisc.edu/networks/ammonia-monitoring-network) and the National Air Pollution Surveillance Program (NAPS, https://open.canada.ca/data/en/dataset/1b36a356-defd-4813-acea-47bc3abd859b). Sulfur dioxide, ozone and NO_x observations are from combined Air Quality System (AQS, https://www.epa.gov/aqs) and NAPS data.

The measurement uncertainty for these networks is given in Table S2 in Section S3 based on acceptance criteria and precision and bias data for AQS, NAPS and AMON. Based on AQS the measurement uncertainty is under 10% for O_3 and SO_2. For NO_2 it is under 15% which falls within the acceptance bound for NAPS. However, AQS and NAPS NO_2 measurements are subject to NO_z interference (Lamsal et al., 2008). The impact is small where NO_x dominates NO_y but can be substantial away from NO sources and dependent on local concentrations of HNO_3 and other NO_y species. For HNO_3 the measurement uncertainty is likely under 15% based on the values provided by McNaughton and Vet (1996) for CAPMoN. CASTNET uses a similar filter pack system. The NH_3 uncertainty falls in the 10-20% range as well.

In the case of ammonia, MOSAIC runs show slightly higher values throughout the year and in all regions with no visible variation in the difference between regions. This is consistent with the lower ammonium levels compared to CAM (see Fig. 11 in the article). Nitric acid shows the most pronounced difference with MOSAIC runs having lower values than CAM runs especially in regions NA1 and NA2. These regions are affected by air masses processed over oceans. The mid-continental region NA4, which has less anthropogenic pollution, has the smallest difference between the two aerosol models. The relatively polluted region NA3 shows an intermediate difference. For either aerosol option the model overestimates HNO_3 for most of the year in regions NA2-4 with late summer and early fall having the largest excess. Region NA1 stands out as having underestimation in summer but an overall better fit to observations over the year compared to the other regions for CAM. The MOSAIC option is biased low compared to CAM and observations in this region.

The additional cation constituents in MOSAIC compared to CAM result in increased uptake of HNO_3 by particulate and subsequent removal by dry and wet deposition. This is especially apparent over the oceans where sea salt sodium forms $NaNO_3$ and HCl is degassed. This leads to lower nitric acid concentrations at the surface over the oceans and regions NA1 and NA2 which experience inland air mass transport. In region NA1 there is predominant transport from the Pacific Ocean due to the prevailing westerlies. Region NA2 is also characterized by substantial transport in spring and summer from the Gulf of Mexico (e.g. Wang et al., 1998). By contrast, region NA3 is in the continental outflow zone over the Atlantic Ocean and experiences sporadic inland transport during coastal storm events. The MOSAIC low bias in HNO_3 and high bias in nitrate (Fig. 11 in the article) in

regions NA1 and NA2 is at least partly linked to the Gong-Monahan sea salt emission scheme which produces excessive sea salt emissions compared to other models and to observations (Spada et al., 2013). However, organics are likely to play a part as well in limiting partitioning of nitric acid into sea salt particulate. Sea salt particles have been observed with substantial organic coatings (e.g. Wang et al., 2017). Such organic aerosol processes are not represented in GEM-MACH.

For either aerosol scheme, the model has substantially less ammonia than observations in all four regions. This can be partially explained by excessive partitioning of NH_3 into the particle phase due to lack of any representation of interference from organic constituents in the aerosol sub-models. But it is likely that agricultural and ocean biogenic emissions of NH_3 are underestimated. The latter is certain since the model has no ammonia emissions over the ocean outside of the Mississippi delta. However, ocean emissions of ammonia are not insignificant (e.g. Paulot et al., 2015, 2020). This will affect region NA1 in particular. Region NA2 is close to the boundary of the model domain which will result in the chemical boundary condition exerting a more pronounced influence than in the case of region NA1.

For SO_2, O_3 and NO_x the difference between MOSAIC and CAM in the REF simulations is too small to see in the figure. This is due to the lack in the model of feedback of aerosols on NO_x concentrations. The model SO_2 is excessive in all regions and for most of the year. Region NA1 shows the largest wintertime bias. This region also differs from the others in having a high bias in wintertime sulfate compared to observations (Fig. 11 in the article). In regions NA2-4 the wintertime sulfur dioxide bias is smaller than in NA1 and this corresponds to a low bias in sulfate. It appears that there is insufficient conversion of SO_2 into sulfate during winter in the model. This putative conversion deficit is reduced in the rest of the year and contributes to the high bias in sulfate seen in summer and fall in regions NA2-4. However, the variation in sulfate from month to month is not simply correlated with SO_2 concentrations and other processes are involved.

The difference between the EMR and REF runs for these gases for both MOSAIC and CAM show essentially no difference and are not shown.

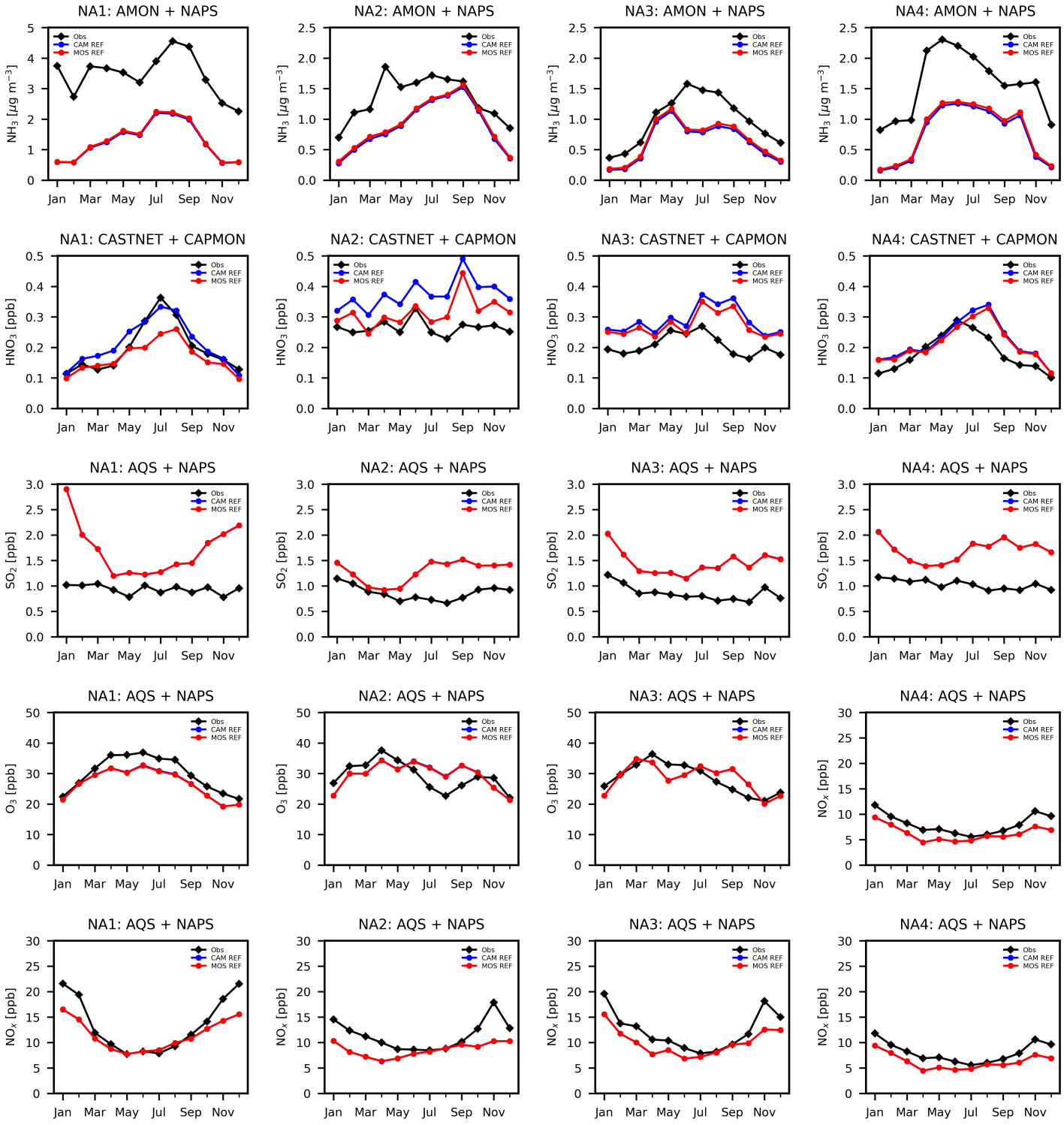


Figure S13: Regional reference run month and station mean time series of NH_3 (1^{st} row), HNO_3 (2^{nd} row), SO_2 (3^{rd} row), O_3 (4^{th} row) and NO_x (5^{th} row). MOSAIC (red), CAM (blue) and observations (black) are shown. Units for NH_3 are $\mu g/m^3$ and for the rest are ppb as dictated by station data.

S3. Ground Station Network Observation Uncertainty

The measurement uncertainty factors for PM2.5 and total PM aerosol species from different observation networks considered in the main article are shown in Table S1. Uncertainty values are not typically available in the distributed station data from any network and is taken from special studies and quality assurance documents. In general, while measurement precision is available for aerosol constituents the bias is not. This is due to a lack of traceable standards for use in the field (McNaughton and Vet, 1996; Solomon et al., 2014). Total measurement uncertainty, TE, is determined by the following expression

$$TE = B + 1.65\,P \qquad (S1)$$

where B is bias and P is precision (Oosterhuis, 2011). For IMPROVE precision and bias are obtained from Table 1 of Hyslop and White (2009) (we use the RMS precision values) (https://aqrc.ucdavis.edu/sites/g/files/dgvnsk1671/files/inline-files/Estimating%20precision%20using%20duplicate%20measurements.pdf). For CSN the bias is assumed to be the same as for IMPROVE and the precision values from Table 15 of Solomon et al. (2014) for 2012 are used. The primary reference for NAPS is Dabek-Zlotorzynska et al. (2011) and specifies an uncertainty under 10% for sulfate, nitrate and ammonium. However, the uncertainty metric is not defined. Hence, we specify the network measurement acceptance criteria which are 15% (see below in this section). For CASTNET the acceptance criteria are given in Table 3-3 of https://www.epa.gov/system/files/documents/2024-06/qapp_v-10-1_main_body_0.pdf. The criteria for 2016 appear to be the same based on general searching of EPA documents. However, these are excessively high given the evaluation by Sickles and Shadwick (2002) who find median coefficient of variation (CV) values of 2.3% for SO_4, 3.7% for NH_4 and 8.1% for NO_3. Bias is estimated to be under 5%. McNaughton and Vet (1996) provide uncertainties that apply for CAPMoN (see their Figure 5 bottom panel). These indicate precision values of ~5% for SO_4 and NH_4 but ~12% for NO_3. Note that absolute precision for CAPMoN sulfate and nitrate is almost the same (~0.06 μg/m^3; Amanda Cole, personal communication). Considering the CVs obtained by Sickles and Shadwick (2002) the CAPMoN NO_3 value is likely under 10% given the use of filter packs in both systems (Sickles et al., 1999). We apply the same 5% bias estimate for CAPMoN on this basis.

Table S1. PM2.5 (CSN, IMPROVE and NAPS) and total PM (CAPMoN and CASTNET) sulfate, nitrate and ammonium measurement uncertainty factors for different ground station networks.

Network	CSN	IMPROVE	NAPS	CAPMoN	CASTNET
SO_4	0.126	0.076	<0.15	<0.133	<0.088
NO_3	0.152	0.136	<0.15	<0.25	<0.184
NH_4	<0.2	-	<0.15	<0.133	<0.111

For gas observations, considered in Section S2, the available uncertainty data is compiled in Table S2. AMON NH_3 uncertainties are obtained from Table 22 of https://nadp.slh.wisc.edu/wp-content/uploads/2021/04/cal_qar_2016.pdf . The uncertainty for AMON NH_3 measurements is

reported by concentration (C) quartile and is a precision metric (lowest to highest: $C < 0.42$, $0.42 < C < 0.94$, $0.94 < C < 1.99$ and $C > 1.99$ $\mu g/m^3$). The overall precision (CV) of Radiello samplers used by AMON was found to be 10% with a systematic low bias of 37% by Puchalski et al. (2011). However, a comparison with CASTNET sites, which used URG annular denuders rather than filter packs to measure NH_3, resulted in a precision (CV) of 5% and low bias of 9% (Puchalski et al., 2015). We use these values to determine the total measurement uncertainty. However, any systematic bias in Radiello samplers should not be included in the total uncertainty since it can be corrected. We do not have any information about such corrected data and use the bias value from Puchalski et al. (2015) as an upper bound. It should be noted that the disagreement between the Puchalski et al. (2011) and Puchalski et al. (2015) studies reflects the small number of non-overlapping stations investigated. The average precision and bias will change when a larger number of stations is considered.

No NAPS gas measurement uncertainty data was found with a literature search. The NAPS data quality criteria specify an accuracy (determined from precision and bias) of 15% or better (https://ccme.ca/en/res/ambientairmonitoringandqa-qcguidelines_ensecure.pdf). The value of 10% for NH_3 for concentrations between 3 and 20 ppb and 20% for values 20 ppb and higher is obtained from Hu et al. (2014).

The AQS acceptance criteria are specified in https://www.epa.gov/sites/default/files/2020-10/documents/app_d_validation_template_version_03_2017_for_amtic_rev_1.pdf. The values of precision (CV) and bias in this document are upper bounds and do not reflect the actual values for different measurement stations. More detailed information is available from single point precision and bias reports (https://www.epa.gov/outdoor-air-quality-data/single-point-precision-and-bias-report). For the state of New York during 2016 the ozone measurement precision was in the range 0.49-4.00% and the absolute bias in the range 0.33-3.32%. Most values were distributed around 1% for both precision and bias. For California during 2016 the precision range was 0.43-5.64% and bias range was 0.55-8.87% with most values below 2.5% for the former and 2% for the latter. The criteria bounds for ozone are 7% for precision and bias but based on these two states the characteristic bounds are less than 3%. Using these lower bounds the total measurement uncertainty is under 8%. For NO_2 typical precision and bias bounds increase to 5% based on the data for these two states. For SO_2 the bounds are 3% for precision and 4% for bias. A full analysis of all stations was not performed and the TE bounds (expression S1) presented here are approximate.

CAPMoN TE bounds are based on McNaughton and Vet (1996) where the precision is taken from their Figure 4. For HNO_3 the relative precision is 6.5% and for SO_2 it is 7.5%. According to this reference the bias is less than 5%.

CASTNET acceptance criteria are specified in Table 2-4 of https://www.epa.gov/system/files/documents/2024-06/qapp_v-10-1_main_body_0.pdf. Total uncertainty values in Table S2 are based on Sickles and Shadwick (2002) who determine a precision of 6.4% for HNO_3 and 4.3% for SO_2. We apply the same 5% bias bound as for CAPMoN since both networks use the same filter pack sampling system. CASTNET measures O_3 with an ultraviolet photometric analyzer and the reference reports a precision of 1.3% and a bias of around 3%.

Table S2. Gas measurement uncertainties by ground station network. For AQS and CASTNET the acceptance bounds are in brackets. NAPS values are acceptance bounds except for ammonia.

Network	AMON[1]	NAPS	AQS	CAPMoN[2]	CASTNET[3]
NH_3	<0.2	0.1-0.2			
O_3		<0.15	<0.08 (0.186)		<0.051 (0.186)
NO_2		<0.15	<0.13 (0.400)		
SO_2		<0.15	<0.09 (0.265)	<0.174	<0.121 (0.265)
HNO_3		<0.15		<0.157	<0.156 (0.348)

1. Puchalski et al. (2015); 2. McNaughton and Vet (1996); 3. Sickles and Shadwick (2002)

Lamsal et al. (2008) show that AQS and NAPS NO_2 measurements can require substantial correction for NO_z interference. Both networks use chemiluminescence analyzers with molybdenum converters. Based on comparison with more accurate photolytic converter measurements, a correction can be applied that reduces unsigned average bias for NO_2. For the Swiss rural station studied this was from 71% to 2.5% in the annual mean. The standard deviation in the bias reduced from around 70% to 30%. NO_z interference is relevant for stations not dominated by local NO_x emissions such as rural stations. Lee et al. (2011) find a 45% average high bias at a Canadian rural site with a strong diurnal variation with the smallest bias during night hours (~15%). There is no correction for this bias in the available network data, and it has to be carried out on a station-by-station basis. The impact of NO_z interference on the model comparison conducted here (Figure S13) indicates that the model is likely biased high rather than low, but the quantification of this is beyond the scope of this research.

S4. Curve Fitting Metrics for Station Network Data

In this section we present more discussion on the similarity metrics used in the network station comparison in Section 4.2. Figure 10 in the main article includes two numbers that measure the fit of model time-series curves compared to observations. The first number measures curve length (Cao and Lin, 2008) and the second measures curve area (Jekel et al., 2019). Smaller values imply a better fit. Table S3 is a tabulation of the values in Figure 10.

For sulfate at rural stations, the EMR MOSAIC case shows the best fit compared to EMR CAM. The Emerson scheme (Emerson et al., 2020) improves both the MOSAIC and CAM scores. The REF MOSAIC case has the worst fit. For nitrate, EMR MOSAIC has the best fit compared to EMR CAM. As with sulfate there is an improvement from the Emerson scheme for both CAM and MOSAIC and REF MOSIAC has the worst fit. Ammonium has a substantially larger error compared to observations relative to sulfate and nitrate. There is an improvement using the Emerson scheme with CAM but not with MOSAIC. However, EMR MOSAIC still shows an improvement over EMR CAM. The reduced scavenging of the fine mode in EMR MOSAIC means more ammonium compared to the REF case. As discussed in our paper, there is a model high bias for ammonium due to lack of inhibition of NH_3 uptake by organics (e.g. Liggio et al., 2011).

For urban stations the metrics for sulfate experience a mixed scoring change with the Emerson scheme. CAM has a degradation of curve length and an improvement in curve area, whereas MOSAIC has a small improvement in curve length and a small degradation in curve area. Overall,

EMR MOSAIC has a poorer fit compared to EMR CAM. For urban nitrate, CAM scores degrade in both metrics in the EMR run compared to the REF run. By contrast, MOSAIC has an improvement in both metrics. Both in the EMR and REF cases, MOSAIC scores worse than REF CAM. Part of the problem for MOSAIC is the high sea salt bias in GEM-MACH which affects coastal stations which have a higher representation from urban sites due to coastal urban clustering. However, urban ammonium for EMR MOSAIC has a noticeably better fit compared to both EMR and REF CAM, even though it is degraded compared to the REF case.

Table S3. Tabulation of similarity metric values from Figure 10 of the article. The first number in each pair is from the metric of Cao and Lin (2008) and the second number is from the metric of Jekel et al. (2019).

Rural				
Species (PM2.5)	**CAM REF**	**CAM EMR**	**MOSAIC REF**	**MOSAIC EMR**
SO_4	0.58, 0.77	0.59, 0.68	0.75, 1.20	0.51, 0.65
NO_3	1.08, 0.92	0.98, 0.89	1.28, 1.11	0.64, 0.53
NH_4	2.17, 2.78	2.00, 2.54	1.43, 1.67	1.79, 2.22

Urban				
Species (PM2.5)	**CAM REF**	**CAM EMR**	**MOSAIC REF**	**MOSAIC EMR**
SO_4	0.55, 0.69	0.60, 0.57	0.62, 0.72	0.59, 0.74
NO_3	0.81, 2.93	0.90, 3.33	1.12, 3.54	1.03, 3.30
NH_4	2.62, 4.49	2.66, 4.56	1.89, 2.83	2.37, 3.74

Rural + Urban				
Species (PM2.5)	**CAM REF**	**CAM EMR**	**MOSAIC REF**	**MOSAIC EMR**
SO_4	0.50, 0.56	0.53, 0.46	0.62, 0.87	0.50, 0.45
NO_3	0.57, 1.05	0.54, 1.03	1.10, 2.11	0.80, 1.51
NH_4	2.58, 4.31	2.60, 4.34	1.84, 2.71	2.31, 3.57

S5. AERONET VSD Uncertainty Analysis and Seasonal Variation

The AERONET VSD data provides measurement uncertainties for the volume median radius (VMR) and standard deviation (SIG) of the fine and coarse mode distributions. Distribution amplitude uncertainty is not provided. For more information see Sinyuk et al. (2020) and https://aeronet.gsfc.nasa.gov/new_web/Documents/U27_summary_final.pdf.

We derive measurement errors for the station averaged VSD distribution based on the measurement uncertainty values for VMR and SIG provided for the collection of stations used in our study. This error data is available for individual measurements which we bin into months. We use the log-normal function given in expression 1 of Roger et al. (2022). The distribution total error, ERR, is based on the absolute value of the partial derivatives of the fine and coarse components of this function with respect to VMR and SIG and evaluated at the central values of these parameters.

$$Fv,c(VMR,SIG)(r) = \frac{dV(r)}{dln(r)} \quad (S2)$$

$$dFv,c = \left|\frac{dFv,c}{dVMR} dVMR(v,c)\right| + \left|\frac{dFv,c}{dSIG} dSIG(v,c)\right| \quad (S3)$$

$$ERR(r) = \sqrt{dFv(r)^2 + dFc(r)^2} \quad (S4)$$

Where F is the volume distribution and subscripts v and c refer to the fine and coarse modes, respectively (expr. S2). The error in F (expr. S4) is determined by the absolute differential of F for each mode (expr. S3).

Figure S14 shows the annual (top right panel) and seasonal (bottom four panels) mean of station averaged AERONET column VSD with vertical error bars specified by the expression above. The horizontal error bars are based on the error in VMR for each mode with the combined distribution values being a weighted blend of the two values at each of the 22 diameters spanning 10 nm to 30 μm. The AERONET VSD inversion has the largest errors in the smallest and largest diameter limits (see Figure 1 in Dubovik et al., 2000). The use of log-normal distributions to invert the VSD from AERONET measurements introduces an error since the actual VSD is not exactly composed of fine and coarse mode log-normal distributions. This error is most apparent as excessively small values in the small-diameter limit of each mode, so that the AERONET VSD values around 10 nm and 1 μm are underestimated. This error cannot be inferred from the VMR and SIG uncertainties and is not captured by the error bars in Figure S14.

The station and monthly mean errors in VMR and SIG for the fine and coarse modes are plotted in the top left panel of Figure S14. The errors are smallest in summer. The fine mode error in both parameters is larger than the coarse mode throughout the year. The spread in error between VMR and SIG is largest for the fine mode with VMR being most uncertain. For the coarse mode the errors are substantially smaller with more overlap between for VMR and SIG values.

The seasonal variation of the model and AERONET volume size distribution is shown in Figure S15. The error bars are monthly standard deviation in each 3-month season. AERONET has the largest VSD in summer and the lowest monthly variation in this season. The model for both the REF CAM and REF MOSAIC options only agrees well with observations in winter. In spring and fall the model has roughly half the VSD amplitude of the observations. In summer this value is around one third. Also, in summer, the model has a coarse mode peak that is smaller than the other seasons and less than the accumulation mode peak, which does not agree with the AERONET pattern of the coarse mode dominating. The smallest difference between the peak values of the coarse and accumulation modes occurs in summer for AERONET.

Although the MOSAIC accumulation mode peak size agrees better with AERONET compared to CAM, the MOSAIC accumulation mode distribution is shifted to smaller sizes in all seasons. This shift is most prominent in winter when the peak size is much smaller. By contrast, the CAM accumulation mode is less pronounced and has a high bias at larger sizes. The CAM accumulation mode peak size agrees with AEORNET and MOSAIC in spring but is too large in summer and fall. For the coarse mode, CAM and MOSAIC have a similar distribution and overlapping peak in winter,

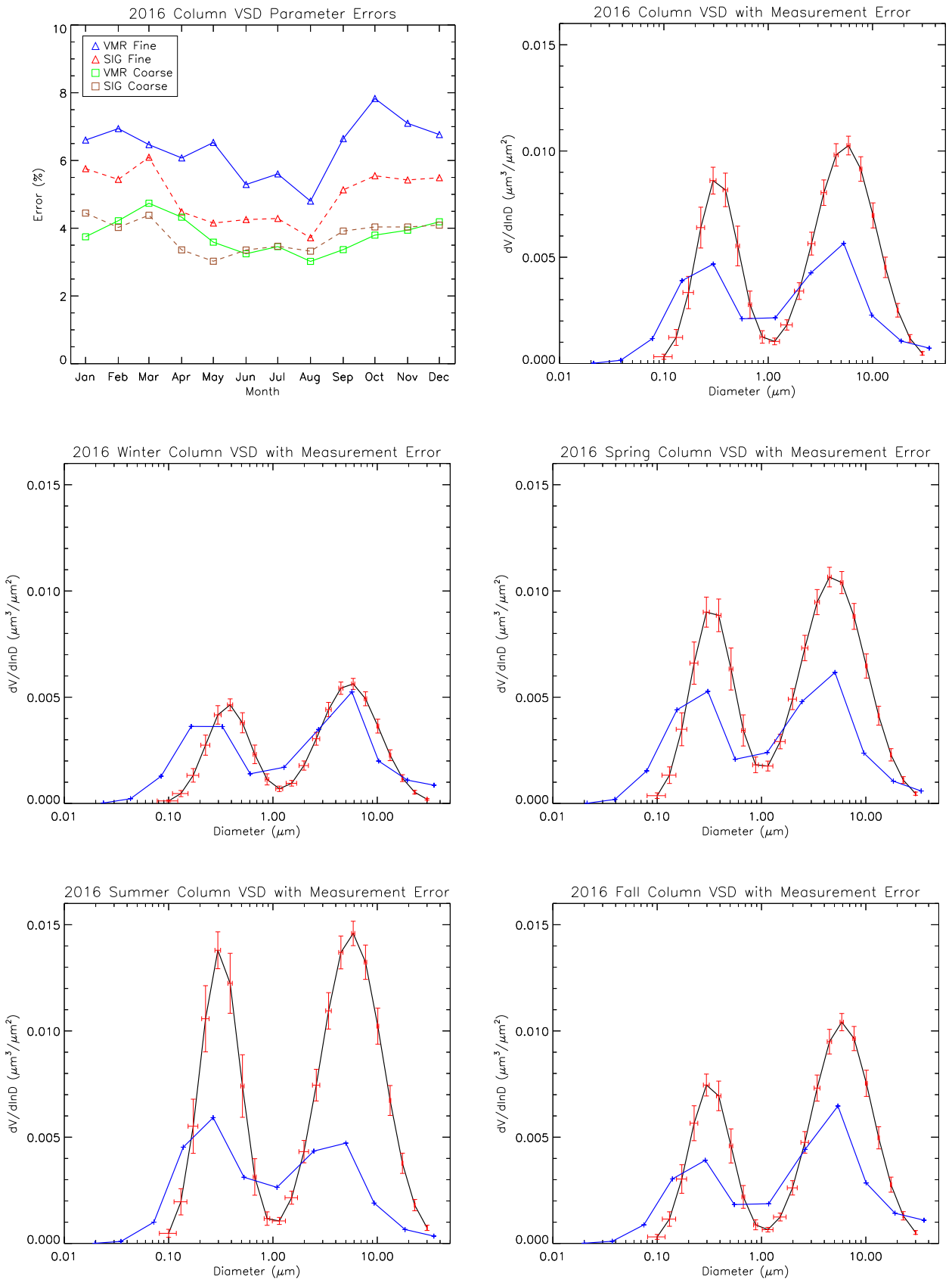


Figure S14: Top left panel: station and monthly mean AERONET U27 errors (in percent) for column VSD size distribution parameters for the fine (triangles) and coarse (squares) modes. The volume median radius (VMR) is shown by solid curves. The standard deviation (SIG) is shown by the dashed curves. Remaining panels: station and time average AERONET column VSD (black) with VMR and SIG derived error bars (red). The annual mean (top right) and seasonal means (bottom four panels) are shown. The REF MOSAIC column VSD is plotted in blue.

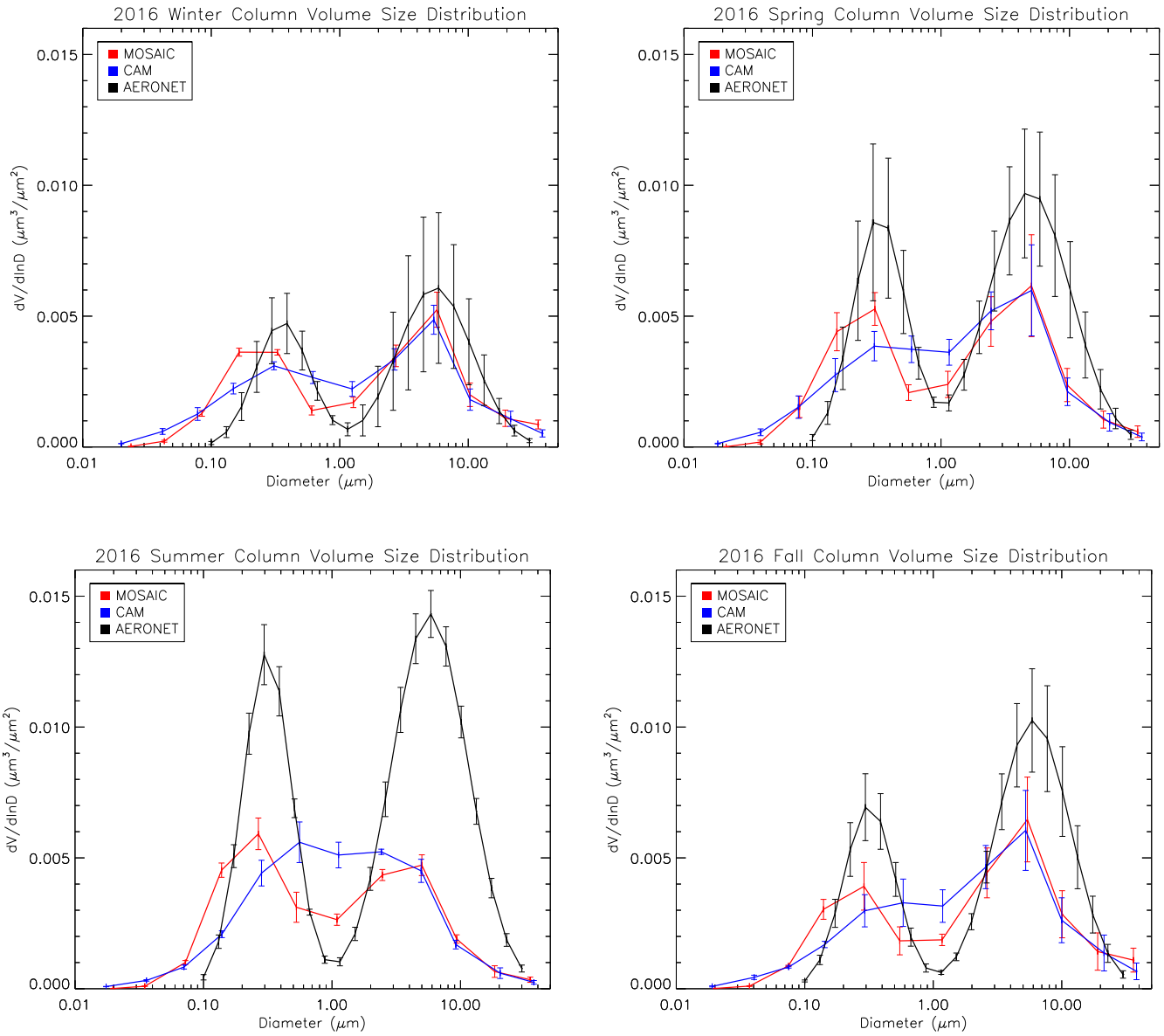


Figure S15: Station and season average VSD for AERONET (black), REF CAM (blue) and REF MOSAIC (red). Error bars are standard deviation using monthly mean data.

spring and fall. However, in summer the CAM coarse mode peak occurs at a smaller size. The CAM VSD is almost unimodal in summer. For both CAM and MOSAIC, the model substantially underestimates coarse mode wet aerosol mass in summer as well as in solstice seasons.

S6. Aerosol Optical Characteristics.

Here we present a comparison of EMR CAM and EMR MOSAIC column aerosol optical depth (AOD), single scattering albedo (SSA) and Angstrom exponent (AE) for the EMR case with AERONET observations. The results from the REF case are very similar and not shown. The calculations are based on the code provided in Appendix A of Bohren and Huffman (1983) as modified by B. T. Draine (https://www.astro.princeton.edu/~draine/scattering.html). This code has been implemented in GEM-MACH previously and does not account for composition and mixing state effects. We use the same AERONET station location aerosol profiles used to produce the column VSD in Section 4.3 of the main article. These profiles are only available once per day in the model output. Therefore, as in Section 4.3, the analysis here should be considered as qualitative.

Figure S16 shows monthly and station mean column AOD and SSA at four wavelengths (440 nm, 675 nm, 870 nm and 1020 nm). The error bars are standard deviation over stations. Column values are calculated as vertical integrals (sum of discrete values multiplied by level thickness) divided by the column depth. The measurement uncertainty for AOD lies within 1-2% (Eck et al., 1999). For SSA the uncertainty lies within 2-3% based on the U27 error data supplied for the AERONET stations considered here. The AERONET data is shown in black, EMR CAM in blue and EMR MOSAIC in red. For 440 nm, the MOSAIC AOD fit compared to CAM degrades in winter but marginally improves in spring and summer. For the other wavelengths, MOSAIC is closer to observations in summer and fall. The model SSA shows too little seasonal variation for both CAM and MOSAIC. Both aerosol schemes have SSA over 0.9 throughout the year, but MOSAIC is closer to 0.9 and fits the observations better in May to July.

SSA is determined by aerosol composition, size distribution and mixing state (e.g. Tian et al., 2023). The more realistic accumulation mode size distribution with MOSAIC appears to explain the improvement compared to CAM. However, the seasonal cycle of the size distribution in CAM and MOSAIC (see Fig. S15) does not explain the lack of substantial seasonal SSA variation. This implies that the model derived SSA using the simple Mie scattering model disagrees with observations due to composition and mixing state differences which are not represented. There is substantial seasonal variation of aerosol composition and mixing state (e.g. Zheng et al., 2021) with winter-time conditions differing from summer-time conditions in terms of hygroscopicity and absorption characteristics. Han et al. (2013) find that SSA is sensitive to the mixing state with a fully mixed state giving the lowest values compared to partially mixed and externally mixed states. By contrast, the AOD is not sensitive to the mixing state. Han et al. (2013) use a more sophisticated aerosol optical properties model (Han et al., 2011) that takes into account mixing state and composition. Since the GEM-MACH model assumes an internal mixture for aerosols, use of a more sophisticated Mie scattering model would reduce the excessive values of SSA during winter by taking into account composition differences.

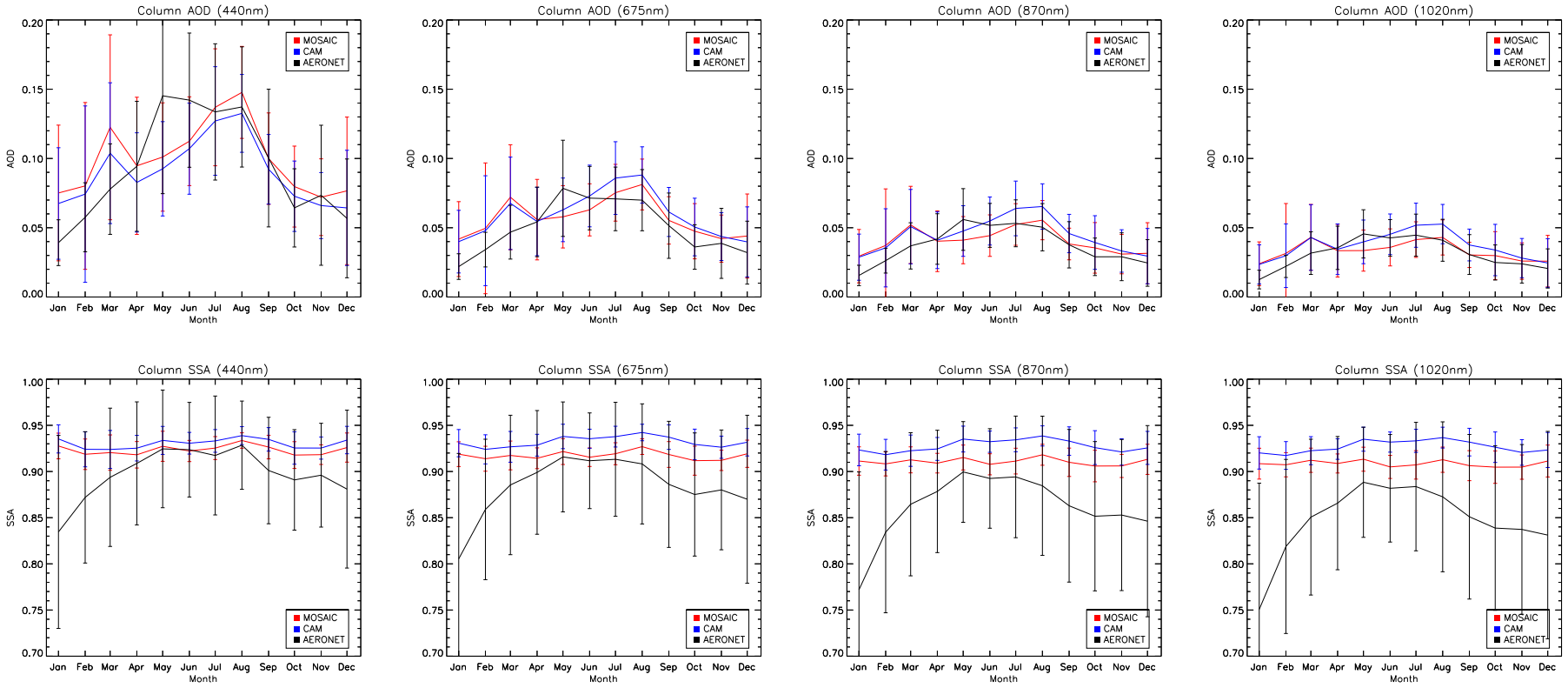


Figure S16: Station and monthly mean column AOD (top panels) and SSA (bottom panels) for 440, 675, 870 and 1020 nm wavelengths. AERONET data is shown in black, EMR CAM in blue and EMR MOSAIC in red. Error bars are standard deviation over stations.

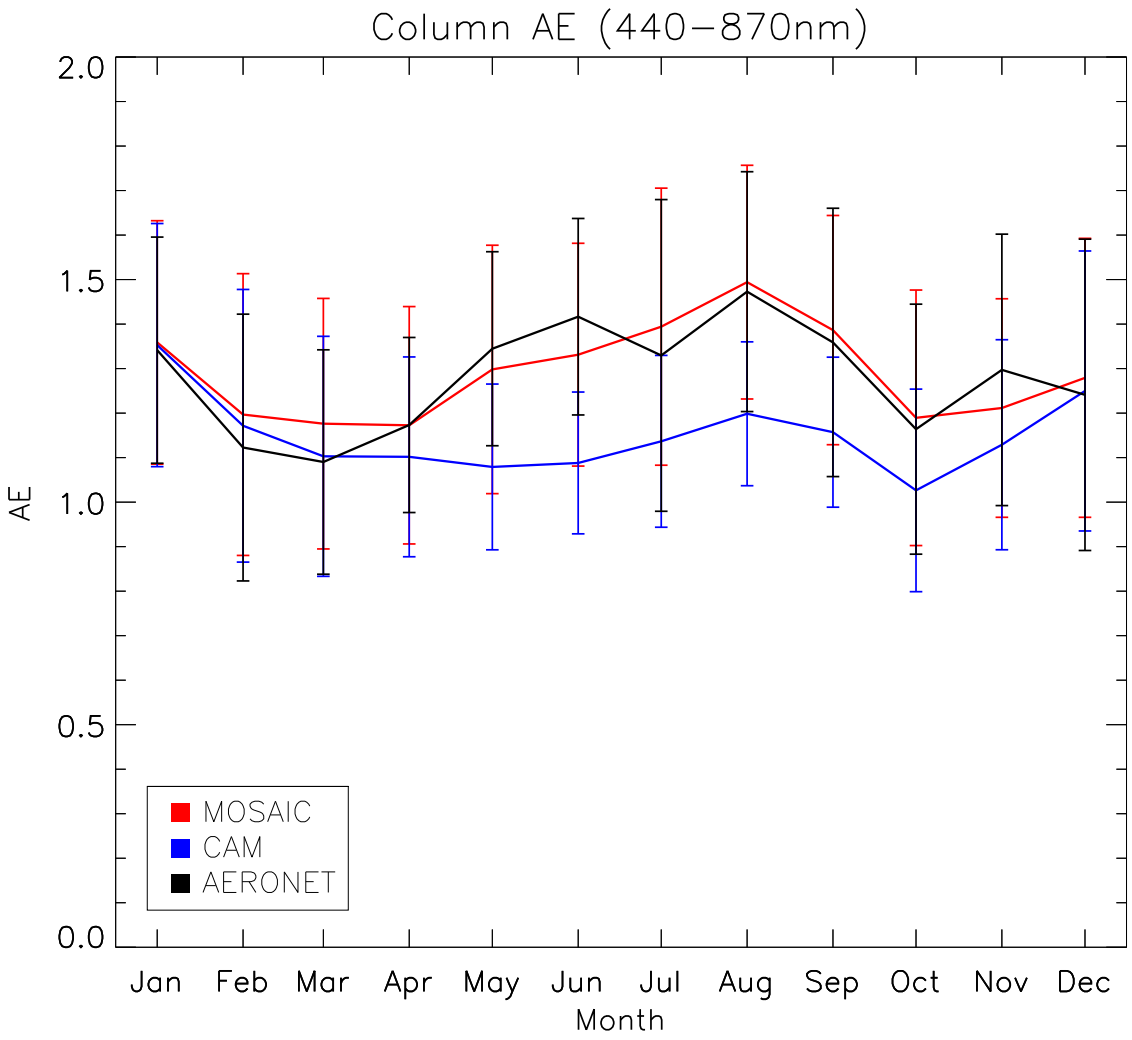


Figure S17: Station and monthly mean column AE (average over 440 - 870 nm). AERONET data is shown in black, EMR CAM in blue and EMR MOSAIC in red. Error bars are standard deviation over stations.

The station and monthly mean column Angstrom exponent (AE) is shown in Figure S17. This value is obtained from the column AOD rather than vertically integrated from profile values. EMR MOSAIC shows a clear improvement over EMR CAM except in March. CAM has values that are too low from April to November. This reflects the poor accumulation mode size distribution in CAM which is too coarse as can be seen in Figure S15 for the REF case (the EMR case is similar and not shown).

SI References

Bohren, C. F. and Huffman, D. R.: Absorption and Scattering of Light by Small Particles, Wiley and Sons, 530 pp., 1983.

Cao, J. and Lin, J.: A study on formulation of objective functions for determining material models, Int. J. Mech. Sci., 50, 193–204, https://doi.org/10.1016/j.ijmecsci.2007.07.003, 2008.

Dabek-Zlotorzynska, E., Dann, T. F., Kalyani Martinelango, P., Celo, V., Brook, J. R., Mathieu, D., Ding, L., and Austin, C. C.: Canadian National Air Pollution Surveillance (NAPS) PM2.5 speciation program: Methodology and PM2.5 chemical composition for the years 2003–2008, Atmos. Environ., 45, 673–686, https://doi.org/10.1016/j.atmosenv.2010.10.024, 2011.

Dubovik, O., Smirnov, A., Holben, B. N., King, M. D., Kaufman, Y. J., Eck, T. F., and Slutsker, I.: Accuracy assessments of aerosol optical properties retrieved from Aerosol Robotic Network (AERONET) Sun and sky radiance measurements, J. Geophys. Res. Atmospheres, 105, 9791–9806, https://doi.org/10.1029/2000JD900040, 2000.

Eck, T. F., Holben, B. N., Reid, J. S., Dubovik, O., Smirnov, A., O'Neill, N. T., Slutsker, I., and Kinne, S.: Wavelength dependence of the optical depth of biomass burning, urban, and desert dust aerosols, J. Geophys. Res. Atmospheres, 104, 31333–31349, https://doi.org/10.1029/1999JD900923, 1999.

Emerson, E. W., Hodshire, A. L., DeBolt, H. M., Bilsback, K. R., Pierce, J. R., McMeeking, G. R., and Farmer, D. K.: Revisiting particle dry deposition and its role in radiative effect estimates, Proc. Natl. Acad. Sci., 117, 26076–26082, https://doi.org/10.1073/pnas.2014761117, 2020.

Han, X., Zhang, M., Han, Z., Xin, J., and Liu, X.: Simulation of aerosol direct radiative forcing with RAMS-CMAQ in East Asia, Atmos. Environ., 45, 6576–6592, https://doi.org/10.1016/j.atmosenv.2011.08.006, 2011.

Han, X., Zhang, M., Zhu, L., and Xu, L.: Model analysis of influences of aerosol mixing state upon its optical properties in East Asia, Adv. Atmospheric Sci., 30, 1201–1212, https://doi.org/10.1007/s00376-012-2150-4, 2013.

Hu, Q., Zhang, L., Evans, G. J., and Yao, X.: Variability of atmospheric ammonia related to potential emission sources in downtown Toronto, Canada, Atmos. Environ., 99, 365–373, https://doi.org/10.1016/j.atmosenv.2014.10.006, 2014.

Hyslop, N. P. and White, W. H.: Estimating Precision Using Duplicate Measurements, J. Air Waste Manag. Assoc., 59, 1032–1039, https://doi.org/10.3155/1047-3289.59.9.1032, 2009.

Jekel, C. F., Venter, G., Venter, M. P., Stander, N., and Haftka, R. T.: Similarity measures for identifying material parameters from hysteresis loops using inverse analysis, Int. J. Mater. Form., 12, 355–378, https://doi.org/10.1007/s12289-018-1421-8, 2019.

Lamsal, L. N., Martin, R. V., van Donkelaar, A., Steinbacher, M., Celarier, E. A., Bucsela, E., Dunlea, E. J., and Pinto, J. P.: Ground-level nitrogen dioxide concentrations inferred from the satellite-borne Ozone Monitoring Instrument, J. Geophys. Res. Atmospheres, 113, https://doi.org/10.1029/2007JD009235, 2008.

Lee, C. J., Brook, J. R., Evans, G. J., Martin, R. V., and Mihele, C.: Novel application of satellite and in-situ measurements to map surface-level NO_2 in the Great Lakes region, Atmospheric Chem. Phys., 11, 11761–11775, https://doi.org/10.5194/acp-11-11761-2011, 2011.

Liggio, J., Li, S.-M., Vlasenko, A., Stroud, C., and Makar, P.: Depression of Ammonia Uptake to Sulfuric Acid Aerosols by Competing Uptake of Ambient Organic Gases, Environ. Sci. Technol., 45, 2790–2796, https://doi.org/10.1021/es103801g, 2011.

McNaughton, D. J. and Vet, R. J.: Eulerian model evaluation field study (EMEFS): A summary of surface network measurements and data quality, Atmos. Environ., 30, 227–238, https://doi.org/10.1016/1352-2310(95)00273-2, 1996.

Oosterhuis, W. P.: Gross Overestimation of Total Allowable Error Based on Biological Variation, Clin. Chem., 57, 1334–1336, https://doi.org/10.1373/clinchem.2011.165308, 2011.

Paulot, F., Jacob, D. J., Johnson, M. T., Bell, T. G., Baker, A. R., Keene, W. C., Lima, I. D., Doney, S. C., and Stock, C. A.: Global oceanic emission of ammonia: Constraints from seawater and atmospheric observations, Glob. Biogeochem. Cycles, 29, 1165–1178, https://doi.org/10.1002/2015GB005106, 2015.

Paulot, F., Stock, C., John, J. G., Zadeh, N., and Horowitz, L. W.: Ocean Ammonia Outgassing: Modulation by CO2 and Anthropogenic Nitrogen Deposition, J. Adv. Model. Earth Syst., 12, e2019MS002026, https://doi.org/10.1029/2019MS002026, 2020.

Puchalski, M. A., Sather, M. E., Walker, J. T., Lehmann, C. M. B., Gay, D. A., Mathew, J., and Robarge, W. P.: Passive ammonia monitoring in the United States: Comparing three different sampling devices, J. Environ. Monit., 13, 3156–3167, https://doi.org/10.1039/C1EM10553A, 2011.

Puchalski, M. A., Rogers, C. M., Baumgardner, R., Mishoe, K. P., Price, G., Smith, M. J., Watkins, N., and Lehmann, C. M.: A statistical comparison of active and passive ammonia measurements collected at Clean Air Status and Trends Network (CASTNET) sites, Environ. Sci. Process. Impacts, 17, 358–369, https://doi.org/10.1039/C4EM00531G, 2015.

Roger, J.-C., Vermote, E., Skakun, S., Murphy, E., Dubovik, O., Kalecinski, N., Korgo, B., and Holben, B.: Aerosol models from the AERONET database: application to surface reflectance validation, Atmospheric Meas. Tech., 15, 1123–1144, https://doi.org/10.5194/amt-15-1123-2022, 2022.

Sickles, I., J. E., Hodson, L. L., and Vorburger, L. M.: Evaluation of the filter pack for long-duration sampling of ambient air, Atmos. Environ., 33, 2187–2202, https://doi.org/10.1016/S1352-2310(98)00425-7, 1999.

Sickles, J. E. and Shadwick, D. S.: Precision of atmospheric dry deposition data from the Clean Air Status and Trends Network, Atmos. Environ., 36, 5671–5686, https://doi.org/10.1016/S1352-2310(02)00723-9, 2002.

Sinyuk, A., Holben, B. N., Eck, T. F., Giles, D. M., Slutsker, I., Korkin, S., Schafer, J. S., Smirnov, A., Sorokin, M., and Lyapustin, A.: The AERONET Version 3 aerosol retrieval algorithm, associated uncertainties and comparisons to Version 2, Atmospheric Meas. Tech., 13, 3375–3411, https://doi.org/10.5194/amt-13-3375-2020, 2020.

Solomon, P. A., Crumpler, D., Flanagan, J. B., Jayanty, R. K. M., Rickman, E. E., and McDade, C. E.: U.S. National PM2.5 Chemical Speciation Monitoring Networks—CSN and IMPROVE: Description of networks, J. Air Waste Manag. Assoc., 64, 1410–1438, https://doi.org/10.1080/10962247.2014.956904, 2014.

Spada, M., Jorba, O., Pérez García-Pando, C., Janjic, Z., and Baldasano, J. M.: Modeling and evaluation of the global sea-salt aerosol distribution: sensitivity to size-resolved and sea-surface temperature dependent emission schemes, Atmospheric Chem. Phys., 13, 11735–11755, https://doi.org/10.5194/acp-13-11735-2013, 2013.

Tian, P., Yu, Z., Cui, C., Huang, J., Kang, C., Shi, J., Cao, X., and Zhang, L.: Atmospheric aerosol size distribution impacts radiative effects over the Himalayas via modulating aerosol single-scattering albedo, Npj Clim. Atmospheric Sci., 6, 1–9, https://doi.org/10.1038/s41612-023-00368-5, 2023.

Wang, H., Wang, X., Yang, X., Li, W., Xue, L., Wang, T., Chen, J., and Wang, W.: Mixed Chloride Aerosols and their Atmospheric Implications: A Review, Aerosol Air Qual. Res., 17, 878–887, https://doi.org/10.4209/aaqr.2016.09.0383, 2017.

Wang, W., Nowlin Jr., W. D., and Reid, R. O.: Analyzed Surface Meteorological Fields over the Northwestern Gulf of Mexico for 1992–94: Mean, Seasonal, and Monthly Patterns, Mon. Weather Rev., 126, 2864–2883, https://doi.org/10.1175/1520-0493(1998)126<2864:ASMFOT>2.0.CO;2, 1998.

Zheng, Z., Curtis, J. H., Yao, Y., Gasparik, J. T., Anantharaj, V. G., Zhao, L., West, M., and Riemer, N.: Estimating Submicron Aerosol Mixing State at the Global Scale With Machine Learning and Earth System Modeling, Earth Space Sci., 8, e2020EA001500, https://doi.org/10.1029/2020EA001500, 2021.